

# Model-Free Source Seeking by a Novel Single-Integrator with Attenuating Oscillations and Better Convergence: Robotic Experiments

Shivam Bajpai, Ahmed A. Elgohary, and Sameh A. Eisa, *IEEE member*

**Abstract**—The classic extremum seeking control (ESC) system has been used, including in experiments, for over a decade as a mean for model-free, real-time method to steer systems, such as mobile robots, to the source of a scalar physical distribution (signal) using only local measurements of said signal. This is referred to in literature as the “source seeking” problem. Similarly, control-affine ESC systems, which are simpler in structure such as single-integrator, have been used for source seeking as well; however, they were rarely experimented on. Both classic ESC and control-affine ESC methods suffer from persistent oscillations even after the system approaches the source they are seeking. In this paper, we implement, and verify by novel robotic experiments, recent results on control-affine ESC, which enable source seeking with attenuating oscillations. We propose a simple, amended single-integrator design which we use in our experiments. The experiments were conducted for a light source seeking problem. Results imply that the proposed design has significant potential as it also demonstrated much better convergence. We hope this paper encourages expansion of the proposed design in other fields, problems and experiments.

**Index Terms**—Source Seeking; Extremum Seeking; Mobile Robot; TurtleBot Experiment; Light Source; Control-Affine

## I. INTRODUCTION

Extremum seeking control (ESC) systems [1] are model-free, real-time adaptive control methods which aim at steering a given dynamical system to the extremum (maximum/minimum) of an objective function [2]. Moreover, the way ESC systems operate make them very desirable to solve many problems in many fields as they only require a perturbation action and measurements of the objective function [2], [3]. That is, ESC systems are operable based on actuating perturbation in a parameter or control input, which then affects the system dynamics, hence, this perturbation is reflected in the measurement of the objective function. Via feedback of said perturbed measurements, the ESC system updates the parameter or the control input to drive the system towards the extremum point. A simple diagram summarizing this idea is provided in figure 1.

Shivam Bajpai is a master’s student in the Department of Aerospace Engineering and Engineering Mechanics, University of Cincinnati, Ohio, USA (e-mail: bajpasm@mail.uc.edu).

Ahmed A. Elgohary is a PhD student in the Department of Aerospace Engineering and Engineering Mechanics, University of Cincinnati, Ohio, USA (e-mail: elgoaam@mail.uc.edu).

Sameh A. Eisa is an assistant professor in the Department of Aerospace Engineering and Engineering Mechanics, University of Cincinnati, Ohio, USA (e-mail: eisash@ucmail.uc.edu).

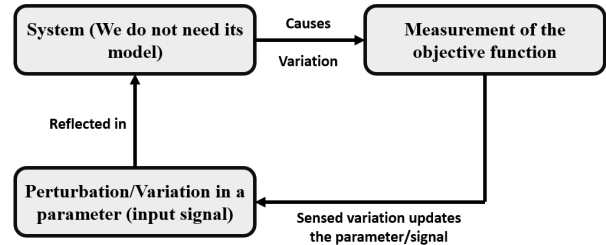


Fig. 1: Simple diagram explaining ESC systems.

Broadly speaking, two types of ESC systems can be found in literature: (i) ESC systems/designs based on the classic structure [4], [5]; and (ii) ESC systems that are in control-affine forms [6], [7]. Both kinds of ESC systems have been applied in unmanned systems, robotics, multi-agent systems, and bio-mimicry (e.g., [2], [6], [8]–[14]). Many of the ESC applications in the mentioned fields fall under what is known as the “source seeking” problem. That is, the ESC system steers a dynamical system (e.g., robot) towards the source point of a signal given that this source represents the maximum/minimum of intensity or strength of said signal. Hence, the ESC advantage in these kinds of problems, i.e., source seeking, is that it will not require the mathematical expression of the signal or its distribution in the spatial domain or any global information for that manner (e.g., GPS). In fact, the ESC source seeking problem is solvable via the local measurement of the signal using, for example, sensors. Hence, ESC systems enable model-free, real-time source seeking. Figure 2 provides the idea of source seeking. However, when it comes to experimental efforts, verification, and deployments, most efforts in literature utilize the classic ESC structure or designs based on it, for the source seeking problem – see for example [15]–[18]. In literature, it is quite rare to find experimental deployments, verification, or efforts involving control-affine ESC structures in general or using them in source seeking; here we cite one of the works were able to find [19] which verifies the theoretical results the same authors have developed in [7].

**Motivation.** Experiments of ESC using robotics, multi-agents, or unmanned systems can be challenging in general. This is due to the continuous oscillations issue in both the control input (e.g., the linear/angular velocity) and around the extremum (usually ESC systems stabilize in a limit cycle, i.e.,

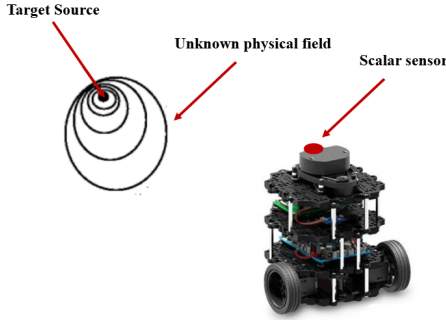


Fig. 2: Sensor-based source seeking

practical stability sense [4], [6], around the extremum). The continuous oscillations in the control input have been shown to be not much of an issue and definitely not an obstacle in real-world experiments of source seeking as shown, for example in [15]–[18]. In fact, we produced experiments using a robot (Turtlebot3) [20] for source seeking of light, replicating the available literature of this problem which use designs based on the classic ESC structure – see our YouTube video [21]. On the other hand, simple control-affine ESC structures can be beneficial to use in the source seeking problem given their overall simpler design, control laws, guaranteed stability [6], [7], and the fact that many of them, like the single-integrator design (see [6]), have much smaller number of parameters to tune compared to many other ESC structures/designs. However, the authors in [19] stated in section IV.B that the control law ( $\dot{x} = u = f(x)\sqrt{\omega}u_1 + \sqrt{\omega}u_2$  where  $u_1$  and  $u_2$  are sinusoidal functions), which is the basis of the simple single-integrator design, performed the “worst” in their experiments. In fact, the same authors showed theoretically in [7] that single-integrator designs with basic quadratic function and sinusoidal control inputs will not achieve asymptotic convergence to the extremum, i.e., they will be persistently oscillating about the extremum.

**Contribution.** In this paper, we take advantage from our recent theoretical developments in [22] which made it possible for control-affine ESC systems, including, simple single-integrator designs, to have attenuating oscillations as the system approaches the extremum point (i.e., asymptotically convergent to the source point in a source seeking problem). In the mentioned work [22], it was shown that structures eminent to have persistent oscillation per [7], [19] can in fact, by *design*, be made structures with attenuating oscillations using what we call Geometric-Based Kalman Filer (GEKF) and an adaptation law which attenuate the control input signals in a stable and adaptive manner so the system perturbs as needed (i.e., the closer the system is from the extremum/source, the smaller perturbation it needs). We aim at using this development to introduce a *novel single-integrator source seeking design with attenuating oscillations*. We provide both simulation results, but more importantly, novel experimental results for source seeking by light. The results show that using the recent theoretical development in [22] one can achieve a model-free, real-

time single-integrator-like source seeking with attenuating oscillations. In fact, our experiments demonstrate that the proposed design possesses *remarkable better convergence*. Our results strongly indicates the potential of our work to be used in other control-affine ESC applications, problems and experiments.

## II. CONTROL-AFFINE EXTREMUM SEEKING WITH ATTENUATING OSCILLATIONS USING GEOMETRIC-BASED KALMAN FILTERING

In this section, we briefly provide the background and preliminaries from our theoretical results in [22] which will be the basis for the main results provided in the next section. Control-affine ESC systems can be characterized by the state space representation (see for example [6], [22]):

$$\dot{\mathbf{x}} = \mathbf{b}_d(t, \mathbf{x}) + \sum_{i=1}^m \mathbf{b}_i(t, \mathbf{x}) \sqrt{\omega} u_i(t, \omega t), \quad (1)$$

with  $\mathbf{x}(t_0) = \mathbf{x}_0 \in \mathbb{R}^n$  and  $\omega \in (0, \infty)$ . Where  $\mathbf{x}$  is the state space vector,  $\mathbf{b}_d$  is the drift vector field,  $u_i$  are the control inputs,  $m$  is the number of control inputs, while the vectors  $\mathbf{b}_i$  correspond to the control vector fields. The control-affine ESC system in (1) can be approximated and characterized by what is known as the Lie-bracket system (LBS) [6], [22]:

$$\dot{\mathbf{z}} = \mathbf{b}_d(t, \mathbf{z}) + \sum_{j=i+1}^m [\mathbf{b}_i, \mathbf{b}_j](t, \mathbf{z}) \nu_{j,i}(t), \quad (2)$$

with  $\nu_{j,i}(t) = \frac{1}{T} \int_0^T u_j(t, \theta) \int_0^\theta u_i(t, \tau) d\tau d\theta$ . The operation  $[\cdot, \cdot]$  donates Lie bracket operation applied to two vector fields  $\mathbf{b}_i, \mathbf{b}_j : \mathbb{R} \times \mathbb{R}^n \rightarrow \mathbb{R}^n$  with  $\mathbf{b}_i(t, \cdot), \mathbf{b}_j(t, \cdot)$  being continuously differentiable, and is defined as  $[\mathbf{b}_i, \mathbf{b}_j](t, \mathbf{x}) := \frac{\partial \mathbf{b}_j(t, \mathbf{x})}{\partial \mathbf{x}} \mathbf{b}_i(t, \mathbf{x}) - \frac{\partial \mathbf{b}_i(t, \mathbf{x})}{\partial \mathbf{x}} \mathbf{b}_j(t, \mathbf{x})$ .

LBSs in (2) as observed in literature (e.g., [6], [7], [22]) are gradient-like systems. They describe qualitatively, and capture the behavior of the control-affine ESC system in (1). In [7], a class of the control-affine ESC system in (1) was proposed to generalize many control-affine ESC systems in the literature (see [7], [22] for more details). Our recent work in [22] extended the mentioned generalized class and proposed a new ESC class which we will use in this paper:

$$\dot{\mathbf{x}} = \sum_{i=1}^n (b_{1i}(f(\mathbf{x})) \sqrt{\omega} a_i(t) \hat{u}_{1i} + b_{2i}(f(\mathbf{x})) \sqrt{\omega} a_i(t) \hat{u}_{2i}) e_i, \quad (3)$$

$$\dot{\mathbf{a}} = \sum_{i=1}^n (-\lambda_i (a_i(t) - J_i(t, \mathbf{x}))) e_i, \quad (4)$$

where  $e_i$  denotes the  $i^{th}$  unit vector in  $\mathbb{R}^n$ . Moreover,  $b_{1i}$  and  $b_{2i}$  are the vector fields associated with the control inputs  $u_{1i} = a_i \sqrt{\omega} \hat{u}_{1i}(\omega t), u_{2i} = a_i \sqrt{\omega} \hat{u}_{2i}(\omega t)$ , the objective function  $f : \mathbb{R}^n \rightarrow \mathbb{R}$ ,  $a_i \in \mathbb{R}$  is the amplitude of the input signal, and  $\lambda_i > 0 \in \mathbb{R}$  is a tuning parameter. Lastly,  $J_i(t, \mathbf{x})$  represents the estimation of the right hand side of the LBS in (2) which can be estimated merely by estimation of the gradient of the objective function  $\nabla f(\mathbf{x})$  as shown in our work [22]. Now, we impose the following assumptions:

- A1.  $b_{ji}, b_{ji} \in C^2 : \mathbb{R} \rightarrow \mathbb{R}$ , and for a compact set  $\mathcal{C} \subseteq \mathbb{R}$ , there exist  $A_1, \dots, A_3 \in [0, \infty)$  such that  $|b_j(x)| \leq A_1, |\frac{\partial b_j(x)}{\partial x}| \leq A_2, |\frac{\partial [b_j, b_k](x)}{\partial x}| \leq A_3$  for all  $x \in \mathcal{C}, i = 1, 2; j = 1, 2; k = 1, 2$ .
- A2.  $\hat{u}_{1i}, \hat{u}_{2i} : \mathbb{R} \times \mathbb{R} \rightarrow \mathbb{R}, i = 1, 2$ , are measurable functions. Moreover, there exist constants  $M_i \in (0, \infty)$  that  $\sup_{\omega t \in \mathbb{R}} |\hat{u}_i(\omega t)| \leq M_i$ , and  $\hat{u}_i(\cdot)$  is T-periodic, i.e.  $\hat{u}_i(\omega t + T) = \hat{u}_i(\omega t)$ , and has zero average, i.e.  $\int_0^T \hat{u}_i(\tau) d\tau = 0$ , with  $T \in (0, \infty)$  for all  $\omega t \in \mathbb{R}$ .
- A3. There exists an  $x^* \in \mathcal{C}$  such that  $\nabla f(x^*) = 0, \nabla f(x) \neq 0$  for all  $x \in \mathcal{C} \setminus \{x^*\}; f(x^*) = f^* \in \mathbb{R}$  is an isolated extremum value.
- A4. Let the estimation error of  $J_i(t, x)$  be  $\eta_i(t)$ , then  $\eta_i(t) : \mathbb{R} \rightarrow \mathbb{R}, i = 1, \dots, n$  is measurable function and there exist constants  $\theta_0, \epsilon_0 \in (0, \infty)$  such that  $|\eta_i(t_2) - \eta_i(t_1)| \leq \theta_0 |t_2 - t_1|$  for all  $t_1, t_2 \in \mathbb{R}$  and  $\sup_{t \in \mathbb{R}} |\eta_i(t)| \leq \epsilon_0$ . Furthermore,  $\lim_{t \rightarrow \infty} \eta_i(t) = 0$ .

The following theorem from our work in [22] provides the stability condition for the the ESC system (3)-(4).

*Theorem 1:* Let A1-A4 be satisfied with some  $\omega \in (\omega^*, \infty), \omega^* > 0$  and suppose  $\exists t^* > t_0 = 0$  such that  $\forall t > t^*$  and  $|J_i(t, z)| \leq 1/t^p$  with some  $p > 1$  then (i) the equilibrium point  $\hat{z}^* \in \mathcal{C}$  is locally asymptotically stable for the estimated LBS of  $\dot{z} = J_i(t, z)$ , (ii)  $a_i$  in (4) is asymptotically convergent to 0; and (iii) the system in (3) is practically asymptotically stable.

The proposed ESC structure in our work [22] for  $n = 1$  is shown in figure 3. Note that for Theorem 1 to be viable, the assumption A4 needs to be satisfied. This has been achieved in our recent results [22] via the use of a novel geometric-based Kalman Filter (GEKF) algorithm which provided a mean, with bounded and attenuating estimation error (to satisfy A4), for estimating the gradient of the unknown objective function  $\nabla f(x)$  in control-affine ESC systems. This enables the estimation of the right hand side of LBS. i.e.,  $J(t, x)$  which then enables the attenuation law to function properly as in (3)-(4) and figure 3.

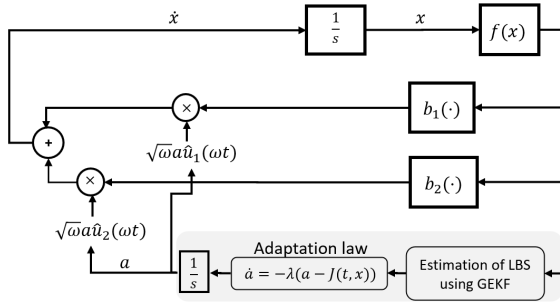


Fig. 3: The proposed ESC design in [22].

### III. MAIN RESULTS

For the experimental work utilized in this section, we use the Turtlebot3 robot. Turtlebot3 (TB3) is a small, affordable, ROS-based, and differential drive mobile robot platform that is designed by ROBOTICS, for the purpose of research, education, and development in the field of robotics [20]. It

has two forms: burger, and waffle. In this work, we have used the burger type which is equipped with sensors, single board computer (Raspberry Pi 3B+), OpenCR, and dynamixel motors. Its wheel base and wheel radius are 160mm and 33mm, respectively [20]. In fact, the robot displayed in figure 2 is a TB3. An overview of the experimental setup is shown in figure 4. There are three main components in the setup which we highlight here for clarity. First component (denoted by #1) is the TB3. Second component (denoted by #2) is the light source utilized during the experiment, which can be replaced by any extremum/source in the context of ESC literature. Third component (denoted by #3) is the motion capture system employed to track and visualize the planar trajectory of the TB3.

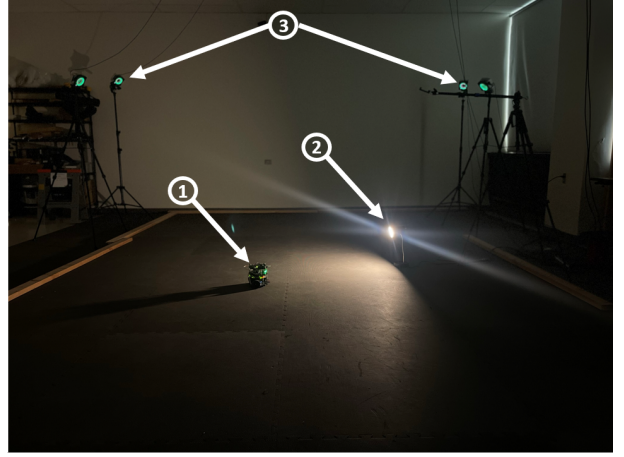


Fig. 4: Overview of the experimental setup.

#### A. Novel Single-Integrator-Based Source Seeking Design

Here we provide details on our proposed novel single-integrator-based source seeking design which stabilizes a system (e.g., robot like TB3) about the extremum/source with attenuated oscillations. Traditional single-integrator designs have been used in literature (e.g., [6]). In this work, we propose a novel and amended single-integrator design based on our recent theoretical developments in [22] which is summarized in the previous section. That is, we propose a single-integrator source seeking design with attenuating oscillations as shown in figure 5. Along the same lines of (3)-(4), the proposed design which operates in a planar mode ( $x$  and  $y$  coordinates) can be represented as follows:

$$\begin{aligned} \dot{x} &= c f(x, y) \sqrt{\omega} u_1(\omega t) + a_x \sqrt{\omega} u_2(\omega t), \\ \dot{y} &= -c f(x, y) \sqrt{\omega} u_2(\omega t) + a_y \sqrt{\omega} u_1(\omega t), \\ \dot{a}_x &= -\lambda_x (a_x - J_x(x, y)), \\ \dot{a}_y &= -\lambda_y (a_y - J_y(x, y)), \end{aligned} \quad (5)$$

Where  $u_1(\omega t) = \sin(\omega t), u_2(\omega t) = \cos(\omega t), f(x, y)$  is the objective function,  $\omega$  is the frequency,  $c$  is a constant,  $a_x, a_y \in \mathbb{R}$  are the amplitude of the input signals for  $x$  and  $y$  states, respectively,  $\lambda_x, \lambda_y > 0 \in \mathbb{R}$  are tuning parameters,

and  $J_x(x, y)$  and  $J_y(x, y)$  represent the estimation of the right-hand side of the lie bracket system such that [22]:

$$\begin{aligned} J_x(x, y) &= \alpha_1 \nabla_{z_x} f(x, y) + \eta_1(t), \\ J_y(x, y) &= \alpha_2 \nabla_{z_y} f(x, y) + \eta_2(t), \end{aligned} \quad (6)$$

with  $\alpha_1, \alpha_2$  are constants and  $\eta_1, \eta_2$  are the estimation error of  $J_x, J_y$ , respectively.

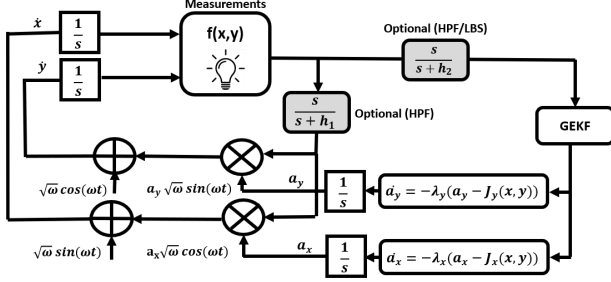


Fig. 5: Proposed amended single-integrator design with GEKF and optional High/Low Pass Filters (HPF/LPS).

As shown in [22], the estimations  $J_x$  and  $J_y$  are good and viable for the validity of Theorem 1 only if the gradient estimation is accurate with vanishing error as  $t \rightarrow \infty$ . This is what we achieved in [22] via the novel filter we called Geometric-based Extended Kalman Filter (GEKF). For our design in this paper, as is the case in [22], GEKF works in real-time and is considered as a discrete-continuous extended Kalman filter that requires: (i) a measurement equation, which is the discrete part that relates the parameter to be estimated (i.e., the gradient of the objective function  $\nabla f(x, y)$  in our case) with measurements we have access to (i.e., measurements of the objective function  $f(x, y)$  in our case); and (ii) the propagation model, which is the continuous part that governs the filter propagation continuously with time between the measurements. The GEKF we have is our design is summarized in Algorithm 1 and explained below. The GEKF states is formulated as follows:

$$\bar{\mathbf{X}} = \begin{bmatrix} \bar{x}_1 \\ \bar{x}_2 \\ \bar{x}_3 \\ \bar{x}_4 \\ \bar{x}_5 \end{bmatrix} = \begin{bmatrix} \frac{K}{2} \nabla_x f(x, y)|_{t_1} \\ \frac{K}{2} \nabla_y f(x, y)|_{t_1} \\ \dot{\bar{x}}_1 \\ \dot{\bar{x}}_2 \\ f(x, y)|_{t_1} \end{bmatrix}_{5 \times 1}, \quad (7)$$

where  $\bar{x}_1$  and  $\bar{x}_2$  are proportional to the gradient components we are estimating. Following the guidelines provided in [22], we take  $k = (2/\sqrt{\omega}) \sin(\omega \Delta t/2)$  where  $\Delta t$  is a short time step between the measurements. Now, following a constant velocity propagation model similar to [22], we get:

$$\dot{\bar{\mathbf{X}}} = \begin{bmatrix} \bar{x}_3 \\ \bar{x}_4 \\ 0 \\ 0 \end{bmatrix}_{5 \times 1} + \Omega \quad (8)$$

where  $\Omega$  represents the process noise as a random variable,  $\mathbf{Q}$  is the covariance matrix for process noise (system noise) and the Jacobian matrix  $\mathbf{A}$  associated with the state dynamics is obtained as

$$\mathbf{A} = \begin{bmatrix} 0 & 0 & 1 & 0 & 0 \\ 0 & 0 & 0 & 1 & 0 \\ 0 & 0 & 0 & 0 & 0 \\ 0 & 0 & 0 & 0 & 0 \\ 0 & 0 & 0 & 0 & 0 \end{bmatrix}_{5 \times 5}. \quad (9)$$

For the measurement updates, The Chen-Flies series expansion is used as shown in detail in [22]. The Chen-Flies expansion can be written as follows:

$$\begin{aligned} f(\mathbf{x}, \mathbf{y})|_{t_2} &= f(\mathbf{x}, \mathbf{y})|_{t_1} + (\nabla f(\mathbf{x}, \mathbf{y}) \cdot \mathbf{b}_1)|_{t_1} K \cos(\omega t) \\ &\quad + (\nabla f(\mathbf{x}, \mathbf{y}) \cdot \mathbf{b}_2)|_{t_1} K \sin(\omega t) + \nu(t). \end{aligned}$$

and

$$\begin{aligned} \mathbf{b}_1 &= [c\sqrt{\omega} f(x, y) \quad ; \quad a_x \sqrt{\omega}], \\ \mathbf{b}_2 &= [-c\sqrt{\omega} f(x, y) \quad ; \quad a_y \sqrt{\omega}]. \end{aligned} \quad (10)$$

where  $t_2 = t_1 + \Delta t$ . The residual terms follow a Gaussian distribution as measurement noise denoted as  $\nu(t) \sim N(0, R)$ , and  $R$  is the covariance matrix associated with noise measurement. Moreover, it is further assumed that the process noise and the measurement noise are uncorrelated. Now, the measurement update equation becomes

$$\begin{aligned} f(\mathbf{x}, \mathbf{y})|_{t_2} &= \mathbf{h}(\bar{\mathbf{X}}) + \nu(t) \\ &= f(\mathbf{x}, \mathbf{y})|_{t_1} \\ &\quad + \left( c f(\mathbf{x}, \mathbf{y}) \nabla_x f(\mathbf{x}, \mathbf{y}) + a_x \nabla_y f(\mathbf{x}, \mathbf{y}) \right) K \cos(\omega t) \\ &\quad + \left( a_y \nabla_x f(\mathbf{x}, \mathbf{y}) - c f(\mathbf{x}, \mathbf{y}) \nabla_y f(\mathbf{x}, \mathbf{y}) \right) K \sin(\omega t) \\ &\quad + \nu(t) \\ &= \bar{x}_5 + 2c\bar{x}_1 \bar{x}_5 \cos(\omega t) + 2a\bar{x}_2 \cos(\omega t) \\ &\quad + 2a\bar{x}_1 \sin(\omega t) - 2c\bar{x}_2 \bar{x}_5 \sin(\omega t) + \nu(t), \end{aligned} \quad (11)$$

where  $t = (t_1 + t_2)/2$ . The Jacobian matrix associated with the measurement update equation is:

$$\mathbf{C} = \begin{bmatrix} 2c\bar{x}_5 \cos(\omega t) + 2a_y \sin(\omega t) \\ 2a_x \cos(\omega t) - 2c\bar{x}_5 \sin(\omega t) \\ 0 \\ 0 \\ 1 + 2c\bar{x}_1 \cos(\omega t) - 2c\bar{x}_2 \sin(\omega t) \end{bmatrix}_{5 \times 1} \quad (12)$$

Our proposed design in figure 5 will be verified by simulations and mostly real-time, real-world experiments. Here we layout our efforts in conducting said simulations and experiments in the next subsections. Whenever possible, we compare our proposed design in figure 5 (amended single-integrator with GEKF and adaptation law for the attenuation of oscillations) vs. the traditionally found single-integrator design in literature (e.g., [6]). The first phase of our verification results is provided in subsection 3.B. In

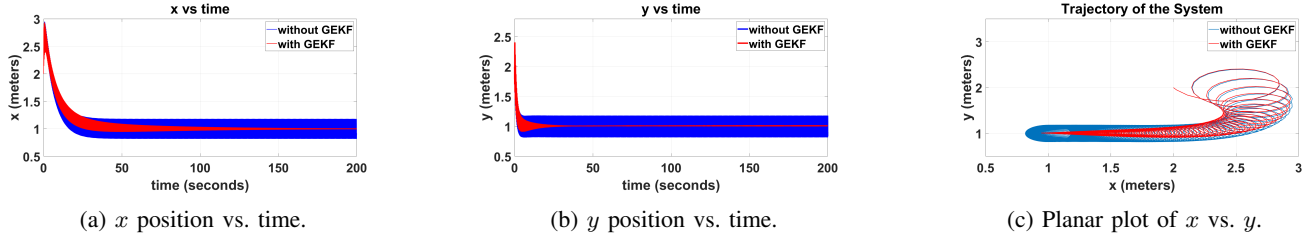


Fig. 6: Trajectories of  $x$  and  $y$  coordinates of the simulation obtaining measurements from a Known objective function simulation. The simulations also compare our proposed design (red), referred to in the legend by “with GEKF” with the literature design (blue), referred to in the legend by “without GEKF.”

---

### Algorithm 1 Geometric-based Continuous-discrete Extended Kalman Filter

---

Initialize  $\bar{X}$  with some initial values.  
choose a sample rate as an output  $T_{out}$  less than the sensors rates (used for measurements ).  
For each sample time  $T_{out}$ :  
for  $i = 1$  to  $N$  do (Prediction Step)  
 $\bar{X} = \bar{X} + (T_{out}/N)\dot{\bar{X}}$   
 $P = P + \frac{T_{out}}{N}(AP + PA + Q)$ ,  
once the measurement is received  $i$  then  
(Measurement step)  
 $C = \frac{\partial h}{\partial \bar{X}}(\bar{X})$   
 $L = PC^T(R + CPC^T)^{-1}$   
 $P = (I - LC)P$   
 $\bar{X} = \bar{X} + L(y[n] - h(\bar{X}))$   
end if

---

that phase, we take the objective function measurements from a mathematical expression which we do not use in any analytical computations (e.g., computing  $\nabla f(x, y)$ ). This enables us to test the design in a more controlled manner and environment. For instance, by taking the measurements from a mathematical expression of an objective function, we can: (i) run a simulation for the experiment before the hardware implementation; (ii) guarantee the applicability of assumptions A1-A3 in the real-world experiment, and (iii) have less noisy environment so that the performance of GEKF is more ideal in its first time ever experimental implementation. The second phase of our verification results is provided in subsection 3.C. In that phase, we take the experiments in a step forward where we use a light sensor for measuring light intensity, aiming at getting the TB3 to achieve a model-free, real-time light source seeking. In this phase, we obviously are working in a complete model-free fashion in all fronts (no equations for TB3 model, sensor, or light intensity/distribution). Lastly, in subsection 3.D, we provide some comments on how Theorem 1 condition seems to have been observed as applicable in our experimentation.

### B. Simulations and Experimentation of the Proposed Design with Known Objective Function

As elaborated at the end of the previous subsection, here we provide details, results and observations of our first phase.

In this phase, we implement our design with a known mathematical expression of the objective function  $f(x, y)$  but only for obtaining measurements. We first present our results via simulations to test and verify the effectiveness of our design. We used MATLAB and Simulink<sup>®</sup> in said simulations. Now, we provide details on the conducted simulations as follows. For the states  $(x, y)$ , the initial conditions are taken as (2,2). For the GEKF, the initial value of the covariance matrix  $P$  is taken as  $[4, 4, 4, 4]^T$ , sample rate  $T_{out} = 0.1$ ,  $Q = 0.05I$  with  $I$  being the identity matrix,  $R = 0.5$  and  $N = 10$ . For the ESC parameters we take  $\omega = 30$ , and  $c = 0.3$ . For the adaptation law we take  $a_x(0) = 1$  and  $a_y(0) = 1$ ; note that for simulations with traditional single-integrator (i.e., no GEKF and no adaptation law),  $a_x = a_y = constant = 1$ ,  $\lambda_x = 0.015$  and  $\lambda_y = 0.0995$ . We used all optional high pass filters (HPFs) such that  $h_1 = h_2 = 1$ . The objective function we used for obtaining the measurements is  $f(x, y) = 10 - \frac{1}{2}(x-1)^2 - \frac{3}{2}(y-1)^2$  which clearly yields an extremum (maximum) at  $f^* = 10$  when  $(x, y) = (1, 1)$ .

The simulation results are provided in figure 6 parts (a)-(c) in addition to figure 8 (top). From part (a) in figure 6, it is obvious that our proposed design with GEKF attenuated the oscillations and asymptotically converged to the maximum point of  $x$ . The same for part (b) where the maximum point for  $y$  was reached with attenuated oscillation. As expected, if we plot  $x$  vs.  $y$  to obtain a planner trajectory of the system (see part (c)), we also achieve convergence with attenuated oscillations. Lastly, the objective function reached its maximum  $f^* = 10$  with attenuated oscillations in figure 8 (top). In all simulations, it is safe to conclude that our proposed design with GEKF outperformed the literature design (no GEKF) significantly in that it converged faster and with attenuated oscillations.

Moving forward with the experimental part of this phase, we conducted real-world experiments in which we used the same known objective function that we used in the simulations for the mere purpose of obtaining measurements. In our experiments, we implemented the proposed single-integrator design with GEKF and compared its performance with the traditional single-integrator of the literature (no GEKF). For the experimental implementation, we used the following parameters. Initial values of  $(x, y)$  states as (2,2), the covariance matrix  $P$  as  $[4, 4, 4, 4]^T$ , sample rate  $T_{out} = 0.1$ ,  $Q = 0.05I$ ,  $R = 0.5$  and  $N = 10$ . The ESC parameters

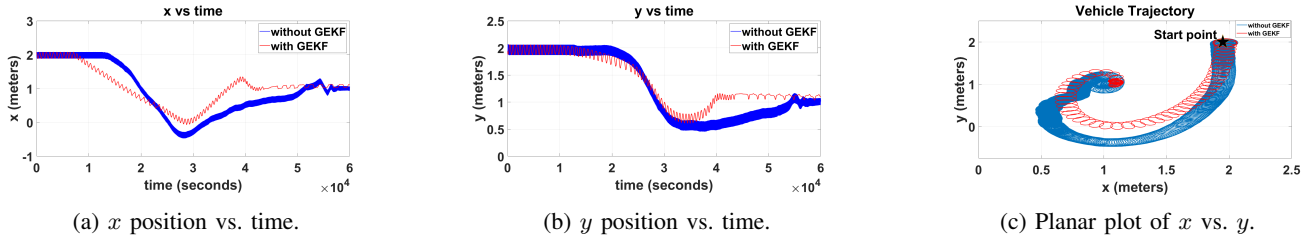


Fig. 7: Trajectories of  $x$  and  $y$  coordinates of the real-world, real-time TB3 robotic experiment obtaining measurements from a known objective function. The data captured for the trajectories via the motion capturing system are presented here. We did the experiment two times to compare our proposed design (red), referred to in the legend by “with GEKF” with the literature design (blue), referred to in the legend by “without GEKF.”

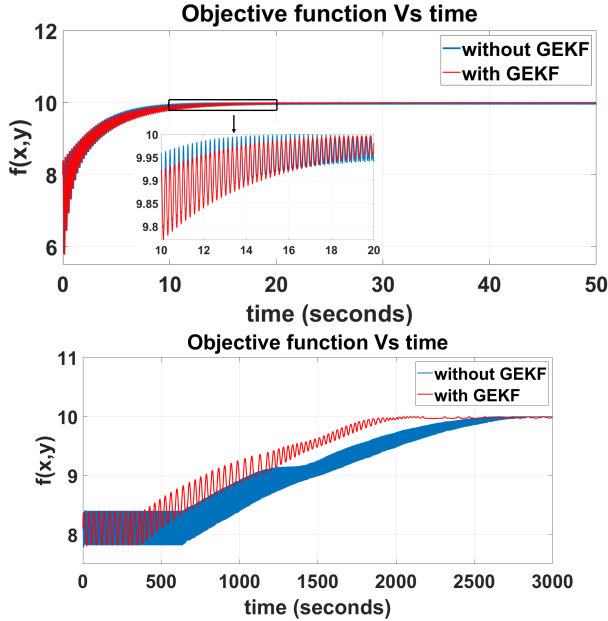


Fig. 8: Objective Function vs. time (top for simulation, bottom for experimental implementation). The proposed design (red) is referred to by “with GEKF” whereas the literature design is referred to by “without GEKF.”

are:  $\omega = 30$  and  $c = 0.5$ . The adaptation law parameters:  $a_x(0) = 0.137$ ,  $a_y(0) = 0.137$ ; note that for simulations with traditional single-integrator (i.e., no GEKF and no adaptation law),  $a_x = \text{constant} = 0.137$ ,  $a_y = \text{constant} = 0.137$ , and the tuning parameter  $\lambda_x = \lambda_y = 0.005$ . The two optional HPF were used such that  $h_1 = h_2 = 0.005$ .

Our real-world, real-time experimental results are presented in figure 7. We can *remarkably* observe the effectiveness of our proposed design for the first time ever experiments involving GEKF. It is clear that  $x$  and  $y$  states reached the desired maximum point with attenuated oscillations (i.e., achieving asymptotic convergence) as shown in parts (a) and (b) of the figure. Moreover, as shown in part (c) of the planar plot, the TB3 reached the maximum position taking a shorter and faster path with *better convergence* than the literature design. Moreover, as shown in figure 8 (bottom), the objective function could reach the optimal value faster and

with *better convergence* with our design when compared with the literature. Also, for the convenience of the reader and for better visualization, we made a YouTube video accessible in [23]. It is worth noting that the attenuation of oscillations and asymptotic convergence is the verification of the effectiveness of our design which is based on our theoretical findings in [22]. However, we here *record* that “*better convergence*” was not something that was studied before; this suggests that GEKF can have more and wider benefits to control-affine ESC systems. Hence, this paper suggests the need for future studies on the wider and broader effects of using GEKF in control-affine ESC systems.

### C. Experimentation of the Proposed Design for Model-free, Real-time Source Seeking of Light

For more verification and validation of the effectiveness of our proposed design, we conducted another phase of experimentation. We conducted real-world, real-time experiments in which we used a light intensity/distribution as the unknown objective function which we only have access to its measurements via a light sensor; clearly, the extremum will be the maximum light intensity which will be the position of the source itself (a source seeking problem). That is, this experiment is totally model-free (no mathematical expression is used for the TB3, sensor, or light intensity/distribution). We implemented the proposed design with GEKF and compared it with another implementation using the literature design (no GEKF) for performance evaluation. During our experiments, we used the following parameters. Initial values of  $(x, y)$  states as  $(0, 2)$ , the covariance matrix  $P$  as  $[4, 4, 4, 4, 4]^T$ , sample rate  $T_{out} = 0.1$ ,  $Q = 0.05I$ ,  $R = 100$ , and  $N = 10$ . The ESC parameters are:  $\omega = 30$  and  $c = 1$ . The adaptation law parameters are:  $a_x(0) = 0.027$ ,  $a_y(0) = 0.027$ , and  $\lambda_x = \lambda_y = 0.005$ . The optional HPFs were used such that  $h_1 = h_2 = 1.5$ . As done in the previous phase, for the experiment without GEKF, we took  $a_x = \text{constant} = 0.027$  and  $a_y = \text{constant} = 0.027$ .

Our novel real-world, model-free, real-time experiments showed *remarkably* promising results in two fronts. First, our proposed design could steer the TB3 to the light source with attenuated oscillations (i.e., with asymptotic convergence) with better performance in  $x$  position as shown in part (a) of figure 9 and in  $y$  as shown in part (b) of figure 9; this is also

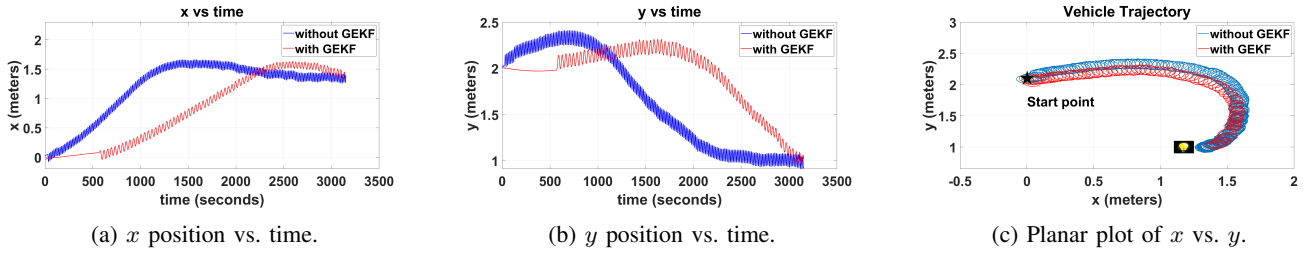


Fig. 9: Trajectories of  $x$  and  $y$  coordinates of the real-world, real-time TB3 robotic experiment obtaining measurements of the light intensity/distribution via sensor. The data captured for the trajectories via the motion capturing system are presented here. We did the experiment two times to compare our proposed design (red), referred to in the legend by “with GEKF” with the literature design (blue), referred to in the legend by “without GEKF.”

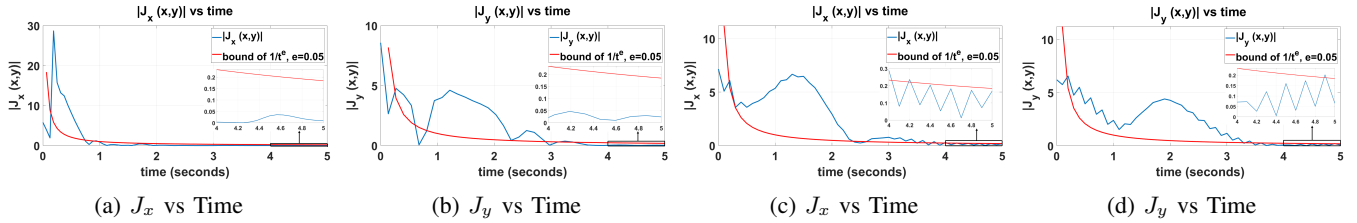


Fig. 10:  $J_x, J_y$  Vs time and bound  $\frac{1}{t^e}$ , (a) and (b) for known objective function experiment, (c) and (d) for light source experiment

clear in the planner plot in part (c) of the same figure. Second, which is, again, an observation we made in the previous phase (subsection 3.B), the TB3 reached the maximum position (the light source itself) taking a shorter and faster path which demonstrates our GEKF design has better *convergence*. It is significant to record here that our proposed design maintained the same observation we made in the previous phase about “better convergence” even though, clearly, source seeking of light via a sensor is less ideal of a condition to experimentation, due to, for example, more noises and sensitivities to the environment. For the convenience of the reader and better visualization, we made a YouTube video for this experiment which is accessible in [24], the first link.

We also conducted another experimentation to further test the capability of the proposed design. It is clear that as the TB3 reaches the light source (the extremum), it will have attenuated oscillations. But what if the light source (the extremum) moves with time (i.e., time varying extremum)? Our adaptation law (see figure 5 and Eq (5)) changes the rate of the amplitude of the input signal depending on how far the system is from the extremum (i.e., the closer the system is from the extremum, the smaller oscillations it needs to extract gradient information). However, from Eq (5), it is clear that the vice-versa situation may be applicable as well. That is, if we start from a small values of  $a_x$  and  $a_y$  and we are far away from the extremum, the adaptation law will increase the rate of  $a_x$  and  $a_y$  to increase the oscillations so that more gradient information can be extracted. Our experiment succeeded in demonstrating the capability of our design to do so and to track the source by increasing or decreasing the oscillations as needed. This suggests that future studies can be done to generalize the results of our work in [22] to admit objective

functions that have time-varying extremum. Our results are provided in figure 11. Also, we made a YouTube video for better visualization that can be accessed in [24], the second link.

#### D. Comments on Stability from Experimentation

In literature, the stability of single-integrator without GEKF has been studied/concluded in [6] and was generalized in [7]. However, for the proposed design with GEKF which is based on the theoretical results provided in our previous work [22], Theorem 1 can be used for verification of stability. Theorem 1 necessitates that the terms  $|J_x(x, y)|$  and  $|J_y(x, y)|$  be bounded eventually after some time  $t^*$  by a decreasing function  $1/t^P$  with  $P > 1$ . Thus, we plotted said components from two experiments: the one from subsection 3.B using the measurements of a known objective function (its results are provided in figure 7); and the one from subsection 3.C using light intensity/distribution measurements via a sensor (its results are provided in figure 9c). The plots show that the components  $|J_x|$  and  $|J_y|$  are behaving as expected per Theorem 1 – see figure 10. Parts (a) and (b) are from the first experiment (figure 7), whereas parts (c) and (d) are from the second experiment (figure 9c).

## IV. CONCLUSIVE REMARKS AND FUTURE WORK

This paper provided a novel design with experimental verification for model free, real-time source seeking via control-affine ESC systems. The paper provided real-world experiments by a robot (TB3) for said design. Experimentation of the proposed design has shown promising results verifying the effectiveness of the significant theoretical developments that have taken place recently in [22] which allows for attenuating the oscillation of the ESC system based on

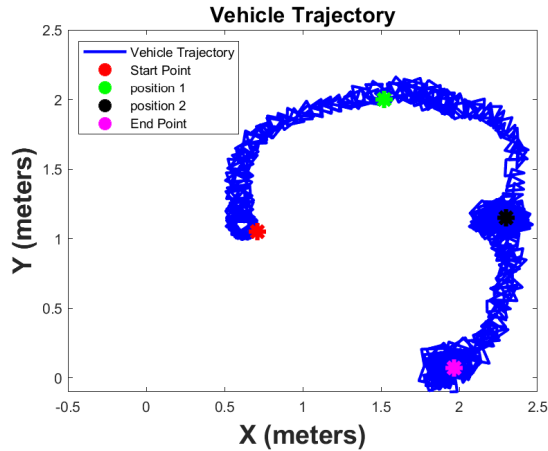


Fig. 11: Planar plot for light source seeking by our proposed design when the source keep changing its position with time. The data captured for the trajectories via the motion capturing system are presented here for the deployed TB3.

what we call Geometric-based Kalman Filter (GEKF). To the best of our knowledge, this paper is the first to provide an experimental validation that single-integrator control-affine ESC systems can perform well. In fact, it was argued and shown in [19] that the simple control laws we used with the single-integrator design ( $\dot{x} = u = f(x)\sqrt{\omega}u_1 + \sqrt{\omega}u_2$  where  $u_1$  and  $u_2$  are sinusoidal functions) are not performing well. This has also been observed in our experiments when we implemented traditional single-integrator of the literature. However, we observed and recorded *remarkable and significant improvement* in performance using our proposed design, which is an amended single-integrator structure with GEKF. Our results concluded that, not only the attenuation of oscillations have been attenuated successfully, but also, the proposed design possesses *better convergence*.

In the future, and encouraged by the results of this paper, multiple studies can take place. First, theoretical analysis should be conducted to provide the necessary conditions and proof that the use of GEKF with control-affine systems improve the convergence. Second, given how successful and effective the use of GEKF have been with simple design and simple control laws of single-integrator, it is recommended justifiably to try amending other control-affine ESC designs using GEKF in a similar manner to this paper. Lastly, it is important to develop a theoretical, and perhaps, experimental works studying the necessary conditions for admitting time-varying objective functions with time-varying extremum to control-affine ESC systems with GEKF.

## REFERENCES

- [1] Y. Tan, W. H. Moase, C. Manzie, D. Nešić, and I. M. Mareels, "Extremum seeking from 1922 to 2010," in *Proceedings of the 29th Chinese control conference*. IEEE, 2010, pp. 14–26.
- [2] K. B. Ariyur and M. Krstic, *Real-time optimization by extremum-seeking control*. John Wiley & Sons, 2003.
- [3] A. Scheinker and M. Krstić, *Model-free stabilization by extremum seeking*. Springer, 2017.

- [4] M. Krstic and H.-H. Wang, "Stability of extremum seeking feedback for general nonlinear dynamic systems," *Automatica-Kidlington*, vol. 36, no. 4, pp. 595–602, 2000.
- [5] M. Krstić, "Performance improvement and limitations in extremum seeking control," *Systems & Control Letters*, vol. 39, no. 5, pp. 313–326, 2000.
- [6] H.-B. Dürr, M. S. Stanković, C. Ebenbauer, and K. H. Johansson, "Lie bracket approximation of extremum seeking systems," *Automatica*, vol. 49, no. 6, pp. 1538–1552, 2013.
- [7] V. Grushkovskaya, A. Zuyev, and C. Ebenbauer, "On a class of generating vector fields for the extremum seeking problem: Lie bracket approximation and stability properties," *Automatica*, vol. 94, pp. 151–160, 2018.
- [8] C. Labar, J. Feiling, and C. Ebenbauer, "Gradient-based extremum seeking: Performance tuning via lie bracket approximations," in *2018 European control conference (ECC)*. IEEE, 2018, pp. 2775–2780.
- [9] S. A. Eisa and S. Pokhrel, "Analyzing and mimicking the optimized flight physics of soaring birds: A differential geometric control and extremum seeking system approach with real time implementation," *SIAM Journal on Applied Mathematics*, pp. S82–S104, 2023.
- [10] M. Abdelgalil, A. Eldesoukey, and H. Taha, "Singularly perturbed averaging with application to bio-inspired 3d source seeking," in *2023 American Control Conference (ACC)*. IEEE, 2023, pp. 885–890.
- [11] C. Zhang, D. Arnold, N. Ghods, A. Siranosian, and M. Krstic, "Source seeking with nonholonomic unicycle without position measurement—part i: Tuning of forward velocity," in *Proceedings of the 45th IEEE Conference on Decision and Control*. IEEE, 2006, pp. 3040–3045.
- [12] S. Zhuo, "Source seeking of multi-uav based on extremum seeking algorithm," in *2017 17th International Conference on Control, Automation and Systems (ICCAS)*. IEEE, 2017, pp. 1062–1067.
- [13] J. Cochran, E. Kansa, S. D. Kelly, H. Xiong, and M. Krstic, "Source seeking for two nonholonomic models of fish locomotion," *IEEE Transactions on Robotics*, vol. 25, no. 5, pp. 1166–1176, 2009.
- [14] J. Cochran, A. Siranosian, N. Ghods, and M. Krstic, "Gps denied source seeking for underactuated autonomous vehicles in 3d," in *2008 IEEE International Conference on Robotics and Automation*. IEEE, 2008, pp. 2228–2233.
- [15] N. Ghods, *Extremum seeking for mobile robots*. University of California, San Diego, 2011.
- [16] T. Xu, G. Chen, G. Zhou, Z. Liu, Z. Zhang, and S. Yuan, "Fast source seeking with obstacle avoidance via extremum seeking control," in *2022 13th Asian Control Conference (ASCC)*. IEEE, 2022, pp. 2097–2102.
- [17] E. A. Bulgur, H. Demircioglu, and H. I. Basturk, "Light source tracking with quadrotor by using extremum seeking control," in *2018 Annual American Control Conference (ACC)*. IEEE, 2018, pp. 1746–1751.
- [18] T. R. Oliveira, N. O. Aminde, and L. Hsu, "Monitoring function based extremum seeking control for uncertain relative degrees with light source seeking experiments," in *53rd IEEE conference on decision and control*. IEEE, 2014, pp. 3456–3462.
- [19] V. Grushkovskaya, S. Michalowsky, A. Zuyev, M. May, and C. Ebenbauer, "A family of extremum seeking laws for a unicycle model with a moving target: theoretical and experimental studies," in *2018 European Control Conference (ECC)*. IEEE, 2018, pp. 1–6.
- [20] ROBOTIS, "Turtlebot3 e-manual," Online. [Online]. Available: <https://emanual.robotis.com/docs/en/platform/turtlebot3/overview/>
- [21] (2023) Light source seeking by the classic structure of extremum seeking control using angular velocity. [Online]. Available: <https://www.youtube.com/watch?v=9seWa-6tggU&t=1s>
- [22] S. Pokhrel and S. A. Eisa, "Control-affine extremum seeking control with attenuating oscillations: A lie bracket estimation approach," in *2023 Proceedings of the Conference on Control and its Applications (CT)*. SIAM, 2023, pp. 133–140.
- [23] (2023) Source seeking by geometric based kalman filtering with control affine extremum seeking. [Online]. Available: <https://www.youtube.com/watch?v=TLom8YMZojg>
- [24] (2023) Source seeking of light by novel extremum seeking design with attenuating oscillation. [Online]. Available: [https://www.youtube.com/watch?v=DTd\\_5bJpxVk](https://www.youtube.com/watch?v=DTd_5bJpxVk), <https://www.youtube.com/watch?v=fM-2Qt3Zldg>